Multi- and Hyperspectral Ocean Color Measurements from Long Island Sound Observation Platform (LISCO): Comparison with Satellite Measurements and Assessments of Uncertainties

Article · May 2011

CITATIONS
0

READS
236

8 authors, including:

Samir A Ahmed
City College of New York
297 PUBLICATIONS **1,919** CITATIONS
SEE PROFILE

Tristan Harmel
French National Centre for Scientific Research
52 PUBLICATIONS **408** CITATIONS
SEE PROFILE

Soe Hlaing
City College of New York
29 PUBLICATIONS **275** CITATIONS
SEE PROFILE

Alberto Tonizzo
Sunstone Scientific
46 PUBLICATIONS **375** CITATIONS
SEE PROFILE

Hyperspectral and multispectral above-water radiometric measurements to monitor satellite data quality over coastal area

Samir Ahmed[1*], Tristan Harmel[1], Alexander Gilerson[1], Soe Hlaing[1], Alberto Tonizzo[1], Curtiss Davis[2], Alan Weidemann[2] and Robert Arnone[2]

[1] Optical Remote Sensing Laboratory of the City College of the City University of New York, NY 10031

[2] Oregon State University

[3] Naval Research Laboratory, Stennis Space Center, MS 39529

*ahmed@ccny.cuny.edu

ABSTRACT

The Long Island Sound Coastal Observational platform (LISCO) near Northport, New York, has been recently established to support satellite data validation. LISCO has both multispectral and hyperspectral radiometers for ocean color measurements. LISCO offers the potential for improving the calibration and validation activities of current and future Ocean Color satellite missions, as well as for satellite intercomparisons and spectral characterization of coastal waters. The multispectral measurements (SeaPRISM system) are part of the NASA AERONET – Ocean Color Network. In addition, LISCO expand observational capabilities for the continuous monitoring and assessment of the hyperspectral (HyperSAS system) and polarized properties Results of measurements made by both the multi- and hyper-spectral instruments, in operation since October 2009, are presented. Intercomparisons between HyperSAS and SeaPRISM data has been carried out, permitting the quantification of the main sources of uncertainty. The three main OCR satellites, MERIS, MODIS and SeaWiFS, have been evaluated against the LISCO dataset of quality-checked measurements of SeaPRISM and HYPERSAS. A first attempt of validation of the hyperspectral imagery provided by the HICO satellite mission is also presented.

Keywords: Ocean Color Radiometry, Coastal Waters, Multispectral, Hyperspectral, Satellite Validation, Satellite Calibration, AERONET-OC

1 Introduction

Optical remote sensing of coastal waters from space is a basic requirement for effective monitoring of global water quality and assessing anthropogenic impacts. However, this task remains highly challenging because of the optical complexity of the atmosphere-water system in coastal areas. Atmospheric correction algorithms are applied to the total satellite signal to remove the contribution of the radiances reflected from the atmospheric and sea surface in order to produce estimates of the exact normalized water-leaving radiances, L_{WN}, the light vertically exiting the water mass under the hypothetical conditions of an overhead Sun and no atmosphere. This geophysical data processing is indeed very sensitive to the atmospheric and water composition as well as to the calibration accuracy of the sensor. The retrieved L_{WN}, which can provide information on the water optical properties and the water composition, is therefore not error free, and its reliability needs to be assessed and validated against actual *in situ* measurements [1]. Consequently, a worldwide effort is devoted to acquiring accurate *in situ* time series measurements in open ocean [2, 3] and coastal waters [4].

In order to support present and future multi- and hyper-spectral calibration/validation activities for Ocean Color Radiometry satellites, as well as the development of new measurements and retrieval techniques for coastal waters, the City College of New York along with the Naval Research Laboratory, Stennis, has established a scientifically comprehensive observational platform, the Long Island Sound Coastal Observatory (LISCO) with multi and hyperspectral radiometry capabilities. The multispectral measurements, obtained by a SeaPRISM system, are part of the NASA AERONET–Ocean Color Network, which has been designed to support long-term satellite ocean color investigations through cross-site consistent and accurate measurements collected by autonomous radiometer systems deployed on offshore fixed platforms making measurements from above water [4-6]. LISCO, complements these multi-

spectral radiometric measurements by additional collocated and continuous hyperspectral measurements using a customized HyperSAS system, which in addition to the spectral radiances measures the hyperspectral polarization properties of these coastal waters [7, 8].

One of the major difficulties of above-water measurements is to correct observations for the impact of reflected sunlight and skylight components [5], which are also randomly fluctuating due to the effect of surface waves. These fluctuations introduce geophysical noise that needs to be removed from SeaPRISM and HyperSAS data, respectively. Based on the retrieval scheme developed for SeaPRISM [4, 9], a hyperspectral-based procedure has been implemented to derive the normalized water-leaving radiance L_{WN} from HyperSAS measurements [10]. Thanks to the ability of LISCO SeaPRISM and HyperSAS to provide two collocated and coincident datasets, the consistency and the efficacy of the above-water data processing were assessed over a period of more than one year encompassing the full natural annual variability of atmospheric and water conditions.

In Section 2, below, the characteristics of the LISCO location and instrumentation are described, and the multi and hyperspectral above-water data correction algorithms detailed. In Section 3, the intrinsic uncertainties of HyperSAS are quantified, based on error propagation throughout the data processing. Then, LISCO data quality is assessed based on the respective data time series of the two collocated multi and hyperspectral systems. The representativeness of LISCO site for satellite validation is discussed. Finally, the three main OCR satellites, MERIS, MODIS and SeaWiFS, have been evaluated against the LISCO dataset of quality-checked measurements of SeaPRISM and HYPERSAS, and a first attempt of validation of the hyperspectral imagery provided by the HICO satellite mission is also presented.

2 Long Island Sound Coastal Observatory (LISCO) Characteristics

2.1 LISCO location

The Long Island Sound Coastal Observatory (LISCO) platform is located at approximately 3 km off-shore in western Long Island Sound, NY, USA. The coordinates of the site are N 40º57'16", W 73º20'30" (Figure 1.a). The bathymetry in the immediate vicinity of the platform exhibits a plateau at around 13 meters depth (Figure 1.b). LISCO is located in the area of western Long Island Sound which is usually moderately turbid with annual average concentrations of Chlorophyll-a and total suspended material of around 12 ± 4 mg m^{-3} and 3 ± 0.5 g m^{-3}, respectively, as estimated by *Aurin et al* [11]. Based on some dozens of field cruises over one year in that region, this recent study qualifies the LISCO waters as very productive and principally driven by phytoplankton biomass and associated detrital materials, rather than suspended sediments. Steady surface currents in the LISCO area are around 0.3 m s^{-1} on average according to NOAA HF Radar dataset.

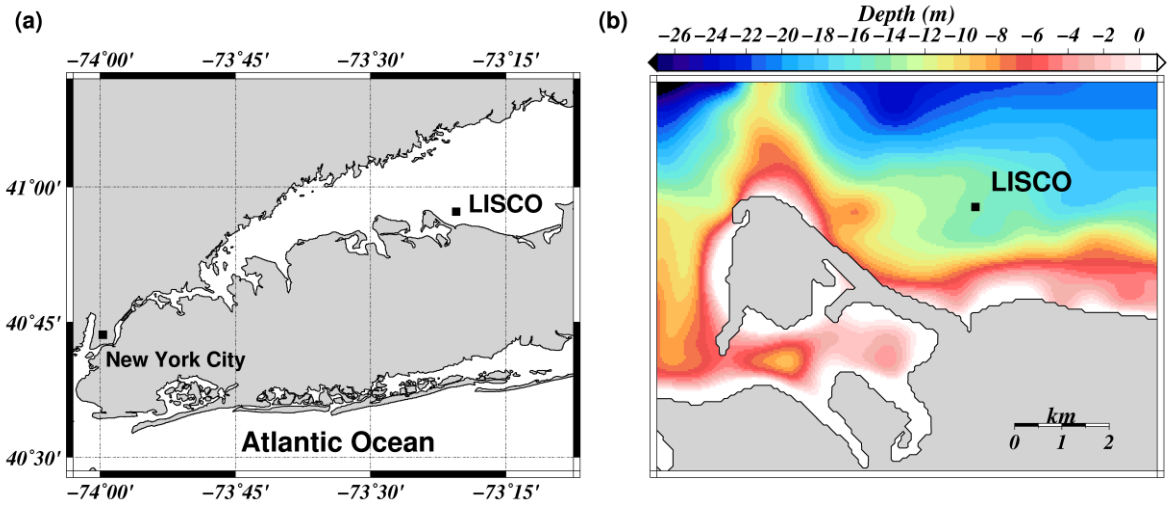

Figure 1. (a) Long Island Sound Coastal Observatory (LISCO) map (LISCO coordinates N40.955°; W73.342°). (b) (Color online) LISCO site bathymetry derived from the General Bathymetric Chart of the Oceans (GEBCO) dataset.

2.2 LISCO instrumentation

The platform combines a multispectral SeaPRISM system (CIMEL ELECTRONIQUE, France) which is now part of AERONET Ocean Color Network [4, 6, 12], with a collocated hyperspectral HyperSAS system (Satlantic, Canada). The instruments are positioned on a retractable tower on the LISCO platform with an elevation of 12 m. Both instruments were installed in October 2009 and have been providing data since then.

The SeaPRISM system is made up of CE-318 sun photometers modified to meet requirements for above-water radiometry. The photometers perform radiance measurements with a full-angle field of view of 1.2° to determine the total radiance from the sea, $L_T(\lambda,\theta,\varphi)$, and the sky, $L_s(\lambda,\theta',\varphi)$, for the relative azimuth angle with respect to the sun φ and the respective viewing angles θ and θ' with $\theta = \pi - \theta'$. Thanks to the rotating feature of SeaPRISM, the azimuth φ is always set to 90° regardless of the sun position; the downwards viewing angle θ is set to 40° from the nadir position. These values were determined in order to minimize both perturbations resulting from the sun glint of the sea surface [13] and the deployment of the superstructure itself or its shadow [6].

The SeaPRISM system configuration of LISCO performs ocean color measurements at the 413, 442, 491, 551, 668, 870 and 1018 nm center wavelengths. These center wavelengths were selected to be as close as possible to the bands of current Ocean Color Radiometry satellite missions in order to support essential validation activities. In addition to these ocean color measurements, the regular data acquisitions of AERONET are also carried out, which permits accurate retrievals of the aerosol optical thickness and the fine-coarse aerosol mode fraction [14].

The hyperspectral measurements are made by a HyperSAS system, providing high precision hyperspectral measurements of total spectral radiance from the sea and the sky as well as downwelling spectral irradiance. The radiance and irradiance measurements of HyperSAS are carried out for 180 spectral channels regularly spaced between 305 and 905 nm. It has two radiance sensors, one looking down at the water, and the other looking skywards. They are mounted at the same location as the SeaPRISM system and each have a full-angle field of view of 3°. Consequently, the sea target sensed by HyperSAS is larger than the SeaPRISM one, indeed the intersection of the field-of-view with the sea surface forms an egg-shape of 0.1 m^2 for SeaPRISM and 0.7 m^2 for HyperSAS. These sensors provide the sea $L_T(\lambda,\theta,\varphi)$ and the sky radiance $L_s(\lambda,\theta',\varphi)$ for a fixed geometrical configuration with $\theta = 40°$ from the nadir view and pointing exactly westwards, as a result the relative azimuth φ is changing with respect to the sun position. Thus, SeaPRISM and HyperSAS point approximately at the same water target area when the Sun is in the South, in other words around 12:00 LT. Each HyperSAS and SeaPRISM sea-viewing measurement sequence is executed every 30 min within plus or minus 4 h of 12:00 LT.

The calibration of the SeaPRISM sun-photometer was carried out by the NASA AERONET group in accordance with the standard procedures of AERONET-OC. The HyperSAS system calibration was carried out by Satlantic, Inc. (Halifax, Canada) and checked at CCNY Optical Remote Sensing Lab. The recalibration of the irradiance sensor have shown a radiometric stability, over a time period of approximately 9 months, of better than 0.5%. SeaPRISM data are transferred by a satellite link to NASA, processed by the NASA AERONET group and posted on the NASA AERONET website. The near-real-time transmission of HyperSAS data is achieved by broadband cellular service to the CCNY server.

2.3 Water-leaving Radiance Retrieval Algorithm

The final geophysical product provided by HyperSAS or SeaPRISM system for their respective spectral bands is the exact normalized water-leaving radiance, L_{WN}, which corresponds to the radiance vertically exiting from the water body just above the sea surface for the ideal case of the Sun at the zenith and no atmosphere [15, 16]. The measured sea radiance $L_T(\lambda,\theta,\varphi)$ can be decomposed into three components: (i) the radiance coming from the direct sun light reflected by the wavy sea surface (sun glint), (ii) the sea surface reflected radiance of the sky light (sky glint) and (iii) the water-leaving radiance emerging from the water body through the sea surface. The data processing aims to retrieve the latter component from the total radiance measured from above water.

For each center wavelength, L_{WN} is retrieved from SeaPRISM measurements by standard NASA processing [4] and from the HyperSAS measurements by a CCNY algorithm based on the same concepts as SeaPRISM data processing. Details on the multispectral data processing can be found in Zibordi et al.[6]; in addition the specificities of the hyperspectral data processing are detailed in Harmel et al.[10].

3 HyperSAS Intrinsic Uncertainty Assessment

A major difficulty with above-water measurements is associated with corrections of observations for the effect of surface waves that introduce significant fluctuations into the glint and reflected skylight components. These fluctuations induce different geophysical noise in respect to the Sun position and viewing geometry [5]. Because HyperSAS and SeaPRISM do not have exactly the same viewing geometry throughout the day, it is of paramount importance to quantify the HyperSAS data quality independently of SeaPRISM. After this initial quality assessment, it will then be possible to make use of HyperSAS and SeaPRISM time series measurements in order to cross-validate both systems.

3.1 Intrinsic Uncertainty Estimator

The data quality assessment of the HyperSAS system, along with its specific data processing procedure, is addressed here. First, all measurement sequences flagged in the HyperSAS data filtering step have been eliminated from the analysis in order to assure the required clear sky condition over the whole dataset. Second, for each measurement sequence, the HyperSAS data processing procedure has been applied to N_T^* sea radiance acquisitions separately, where N_T^* is equal to the 20% of the N_T sea-radiance measurements exhibiting the lowest radiance levels. It should be reminded that N_T varies from 44 to 210 within a measurement sequence of 3 minutes. In addition, it should be noted that this elimination of the highest sea-radiances is equivalent to the effective removal of sun glint effects in the HyperSAS data processing. Thus, N_T^* values of the exact normalized water-leaving radiance L_{WN} are retrieved for each HyperSAS measurement sequence, and it is from these L_{WN} values that an estimator of the relative standard deviation is calculated as follows:

$$\sigma_{rel} = \frac{1}{L_{WN}^{est}} \sqrt{\frac{1}{N_T^* - 1} \sum_{i=1}^{N_T^*} \left(L_{WN}(i) - L_{WN}^{est} \right)^2} \tag{1}$$

where L_{WN}^{est} is the exact normalized water leaving radiance estimated by the operational HyperSAS processing which, as discussed above, makes use of the mean value of the N_T^* sea-radiance measurements as an input. Thus, the value of σ_{rel} is an estimator of the uncertainties induced by the geophysical noise (i.e. environmental effects) and propagated through the whole data processing. This value is used to quantify the geophysical uncertainty of the HyperSAS system.

3.2 HyperSAS Intrinsic Uncertainties

The parameter σ_{rel} has been computed for all the center wavelengths for all the measurement sequences for the different seasons of the year. A synoptic view of HyperSAS intrinsic uncertainties can be expressed by plotting the mean σ_{rel} in respect to the viewing geometrical configuration. This configuration is totally described by the solar zenith angle and the relative azimuth φ between the Sun and the sensor while the HyperSAS viewing angle is fixed and set to 40° from the nadir direction. The convention used for the relative azimuth is φ = 0° when the sensor is in opposition to the Sun, and φ = 180° when the Sun is behind the sensor. The results are displayed in Figure 2 for three center wavelength widely used in ocean color radiometry applications: 443, 550 and 670 nm.

For these three bands, results show minimum uncertainties around φ = 130° which is consistent with previous theoretical studies [13]. The contamination by environmental effects of the retrieved L_{WN} becomes sensitive for φ < 60° whatever the Sun elevation with uncertainties higher than 5%. As a consequence, it has been decided to eliminate from the HyperSAS data quality processing, all data taken for φ < 70°. For the rest of the viewing configurations, the uncertainties remain lower than 5%, thereby showing a large range of viewing configuration available for acquiring accurate water-leaving radiance from above water. Furthermore, it should be noted that no data selection restrictions were made based on wind speed or sea state considerations for the results shown in Fig.4. While the average data quality remains accurate, it can be concluded that the correction scheme of the sea surface effect is sufficiently accurate at the level of 5% uncertainty in L_{WN}. However, it should be remembered that potential biases affecting L_{WN} are not taken into account in this analysis, the only means for quantifying them being comparisons against long time series of collocated measurements, that can be achieved by comparisons with SeaPRISM data, as shown in the next section, or against accurate below-water measurements which are beyond the scope of this paper. In conclusion, the significant HyperSAS data accuracy has been shown on the basis of statistics of daily measurements gathered over more than one year (i.e. October 2009 until January 2011, see Harmel et al.[10] for a discussion on the seasonal variations of this accuracy) exhibiting uncertainties below 5% within consistent spectral and time ranges which are suitable for ocean color radiometry satellite validation activities.

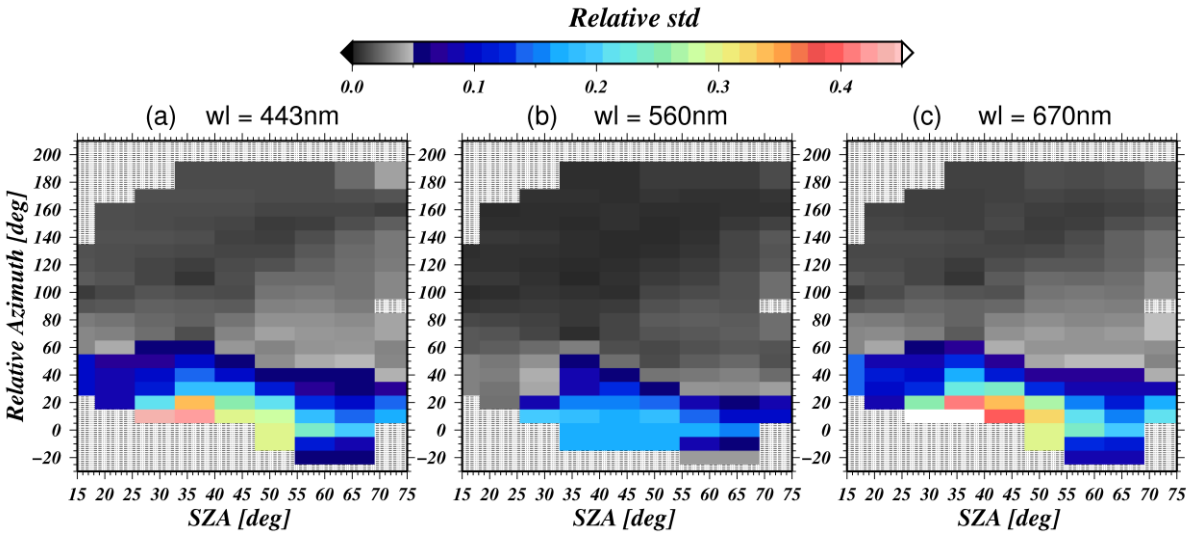

Figure 2. (Color online) Relative standard deviation (uncertainty estimator) of L_{WN} as retrieved by HyperSAS system in respect to the solar zenith angle (SZA) and the relative azimuth between the Sun and the sensor (equal to 180° when the Sun is behind the sensor) at (a) 443, (b) 560 and (c) 670 nm. A gray pattern is used when no data are available.

4 SeaPRISM / HyperSAS Intercomparison

4.1 Water-leaving Radiance Qualitative Intercomparison

Based on the CCNY data processing, the exact water-leaving radiances, L_{WN}, are retrieved from the HyperSAS measurements over a more than one year period. SeaPRISM and HyperSAS data are compared assuming that both systems on the LISCO platform observe the same geophysical target, i.e. the same water composition, at the same time. As an example, the distributions of L_{WN} retrieved from SeaPRISM and HYPERSAS measurements, respectively, are displayed for November 4th 2009 (Figure 3). This comparison shows a satisfactory spectral agreement between the two datasets. In addition, it should be noted that the hyperspectral data exhibit consistent supplementary information, in agreement with other datasets [17], showing specific fine spectral features not discernible in the multispectral L_{WN} data obtained from SeaPRISM.

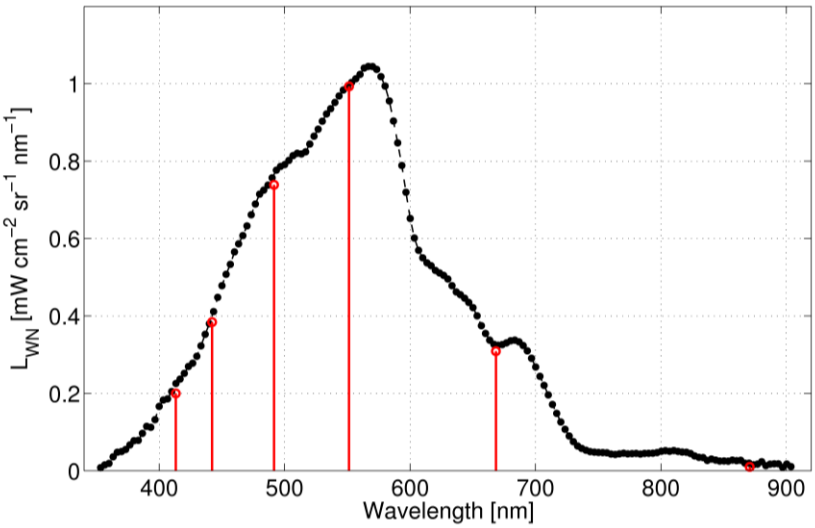

Figure 3. (Color online) Examples of coincident HYPERSAS (black dots) and SeaPRISM (red circles) exact normalized water-leaving radiance (in mW cm^{-2} sr^{-1} nm^{-1}) for November 4th 2009

The whole time series of L_{WN} at two SeaPRISM spectral bands are plotted in Figure 4, including the SeaPRISM and HyperSAS values derived from the quality-checked measurements taken between 9:00 and 16:00 LT. In addition, all the

HyperSAS values with a relative azimuth smaller than 70° have been eliminated because of the glint contamination as shown in the previous section. For each day, the mean value and the standard variation are calculated for SeaPRISM and HyperSAS respectively, and plotted in Figure 4.

In this figure, the time series exhibit strong seasonal variations for both datasets. For instance, a specific pattern of high water-leaving radiances is observable on March 17th 2010 resulting from an increase of sediment concentration following a significant storm event due to higher riverine input and water body mixing. As a result, it can be concluded that the seasonal changes are well captured by the two above-water measurement systems over the 1-year datasets of collocated acquisitions at LISCO site. This temporal agreement combined with the spectral shape agreement of the LISCO data enables to qualitatively validate the concept and the scientific consistency of measuring water-leaving radiance from above water in coastal water area.

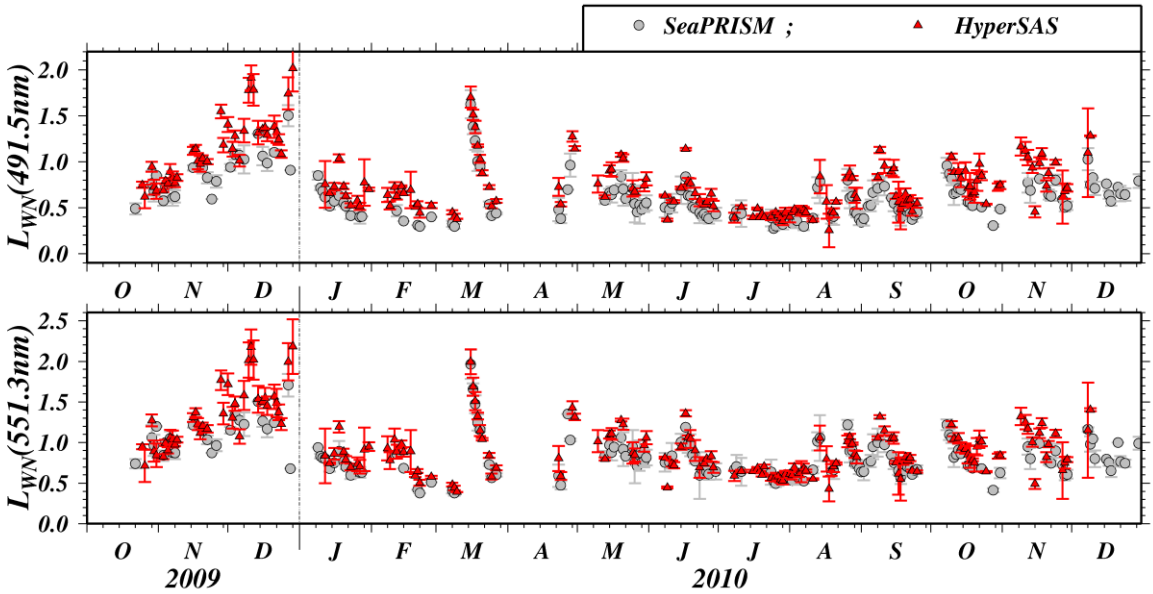

Figure 4. (Color online) Time series of daily average of the exact normalized water-leaving radiance (in mW cm^{-2} sr^{-1} nm^{-1}) retrieved with HyperSAS (red triangles) and SeaPRISM (grey circles) for two SeaPRISM bands centered on 551 and 491 nm. The vertical bars correspond to the daily standard deviations.

4.2 Sources of Uncertainty

To further quantify the uncertainty of the L_{WN} obtained by above-water instrumentation, matchup intercomparisons were used for the whole set of data measured or obtained by SeaPRISM and HyperSAS systems. The intercomparisons were carried out for the four main SeaPRISM spectral bands, i.e. 442, 491, 551 and 668 nm. The hyperspectral HyperSAS data were integrated with the sensor relative spectral response function of each SeaPRISM bands in order to produce equivalent data for both systems. The data involved were restricted to SeaPRISM measurement sequences taken within ±10 min of HyperSAS sequence intervals. Since the sequence interval is 30 min for both systems, the intercomparisons were exclusively achieved between single sequences.

The statistical approach adopted here is associated with the consideration that neither SeaPRISM nor HyperSAS system can be assigned as reference since both systems are in above-water configuration. For this reason the intercomparisons were conducted using the unbiased relative percent difference (URPD) defined as follows:

$$URPD = 200 \times \frac{1}{N} \sum_{i=1}^{N} \frac{y_i - x_i}{x_i + y_i} \tag{2}$$

with x stands for SeaPRISM data and y for HyperSAS data, N being the number of matchup points available. Based on the same notation, the following bias was also used:

$$bias = \frac{1}{N}\sum_{i=1}^{N} y_i - x_i \quad (3)$$

A least squares fit is also adjusted within the matchup points, with the associated coefficient of determination, R^2, and the equation of the regression line. It should be noted that no statistical filtering has been applied to the following intercomparisons to remove outliers.

As it has been shown in Harmel et al.[10], the impact of the successive processing steps on the retrieval uncertainties can be summarized as follows: (i) the sun glint removal step generates unbiased uncertainties of about 2.5%, with a slight positive bias in HyperSAS data, (ii) the sky glint removal step generates unbiased uncertainties of about 6%, (iii) the viewing angle dependence correction improves the data intercomparison by reducing the unbiased uncertainties by more than 1.5%, (iv) the atmospheric effect normalization generates approximately 5% of unbiased uncertainties, and induces a non-negligible bias, especially at the shorter wavelength, most likely due to an insufficiently accurate atmospheric transmittance derivation in the SeaPRISM processing. Ultimately, the exact normalized water-leaving radiances were then retrieved with an overall uncertainty of 19.5% and a positive bias of about 0.09 mW cm^{-2} sr^{-1} nm^{-1} in HyperSAS data (Figure 5). Spectrally, the minimum uncertainty of about 8% occurs at 551nm where the water-leaving signal is high in comparison to the atmospheric one (see Table 1). This uncertainty increases with decreasing water-leaving signal with a URPD value of about 20% at 668nm and greater than 30% in the extreme blue part of the spectrum. In spite of these uncertainties, the HyperSAS and SeaPRISM datasets are strongly correlated for the central wavelengths from 442 to 668 nm (R^2>0.93) and to a lesser extent for the 412 nm band (R^2>0.76) with the slope of the regression lines close to one (Table 1). Based on this result, it can be concluded that the LISCO data provided by collocated above-water instrumentations are statistically satisfactory consistent. They thereby demonstrate effective cross-validation of both HyperSAS and SeaPRISM systems in coastal waters. It should be also noted that the presence of two independent systems on the platform significantly improves quality control. Indeed, the absence of the noticeable trends in correlations and biases between the two instruments minimizes the necessities for instruments' maintenance and recalibration which can introduce additional uncertainties and gaps in the data time series.

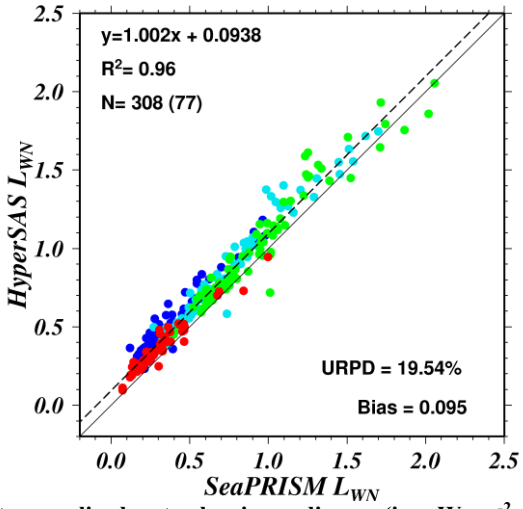

Figure 5. Intercomparison of the exact normalized water-leaving radiances (in mW cm^{-2} sr^{-1} nm^{-1}) derived from SeaPRISM and HYPERSAS measurements for the following center wavelengths 442 nm (dark blue), 490 nm (light blue), 551 nm (green), 668 nm (red).

Table 1. Summary of the intercomparison of HyperSAS and SeaPRISM exact normalized water-leaving radiances L_{WN} over one year period at LISCO site corresponding to 77 coincident measurement sequences.

	Wavelength (nm)					Spectral Average[a]
	412	442	491	551	668	
R^2	0.77	0.92	0.96	0.93	0.93	0.96

Regression line	0.91x+0.13	1.06x+0.11	1.03x+0.09	0.99x+0.09	0.88x+0.09	1.00x+0.09
UPRD	47.7	33.7	15.3	8.4	20.6	19.5

[a] with the exception of 412 nm because of the very low water-leaving signal at this wavelength

5 OCR satellite validation

5.1 Satellite Data Validation based on Multispectral AERONET-OC Data

In order to compare satellite and *in situ* data, the SeaPRISM and HyperSAS data correspond to the values derived from quality-checked measurements (level 1.5) and CCNY quality control[10], respectively. Only the data acquired between 14:30 and 18:30 UTC (i.e. ~10:00 and ~14:00 LT) are considered in the following data comparison. The mean and standard deviation values of the satellite data have been calculated within a 3km×3km area over the LISCO platform. The extreme southwest pixel corresponds to the nearest pixel to the platform. The Ocean Color Reprocessing 2009 has been used to carry out the atmospheric corrections in a unique way for the three main OCR satellite imageries: MERIS (high spatial resolution), MODIS (Aqua, medium spatial resolution) and SeaWiFS (Merged Local Area Coverage data). The quality flags (glint, cloud, high solar and viewing zenith angle, atmospheric correction failure) have been applied for filtering the satellite data; the average values are considered qualified for comparison with in situ data when at least 90% of the pixels are not affected by these standard flags. In addition, more than 20% of pixels within a radius of 10 km of the platform have been eliminated because of cloudiness from the comparison avoiding stray light contamination due to very bright clouds.

The time series of the remote sensing reflectances (R_{rs}) derived from satellite and field measurements are displayed in Figure 6. It can be readily discerned in this time series that the satellite data are varying accordingly to the *in situ* data. In addition, specific patterns of the R_{rs} temporal variations can be seen as for instance the remarkably high water-leaving radiances on March 17th 2010 resulting from an increase of sediment concentration following a significant storm event.

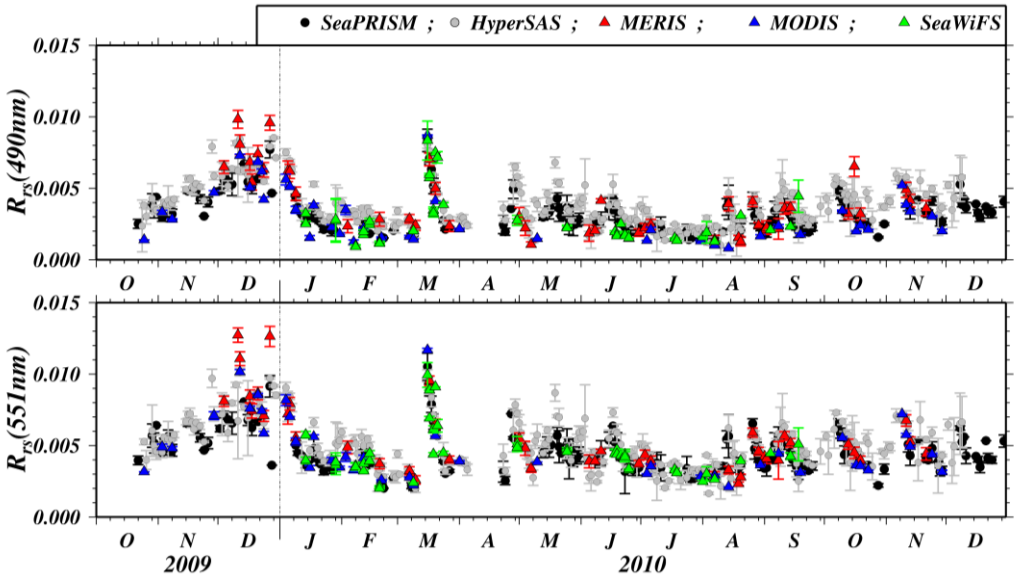

Figure 6. Time series of remote sensing reflectance in sr^{-1} as measured by SeaPRISM (black dots), HyperSAS (gray dots), MERIS (red triangles), MODIS (blue triangles) and SeaWiFS (green triangles) at the spectral bands closest to 490 and 551 nm, respectively.

The satellite data are plotted for matchup comparisons against the SEAPRISM and HYPERSAS data in Figure 7 and Figure 8, respectively. In addition, the absolute percentage difference, APD, and the absolute difference, AD, have been calculated in order to assess the consistency between satellite and in situ R_{rs} as follows:

$$APD = \frac{1}{N}\sum_{i=1}^{N}\frac{|x_i - y_i|}{x_i}, \qquad AD = \frac{1}{N}\sum_{i=1}^{N}|x_i - y_i| \tag{4}$$

with x taken for SeaPRISM data and y for satellite data, have. The regression lines slope close to one along with strong coefficients of determination for wavelength greater than 490 nm. This demonstrates the capacity for monitoring water-leaving radiance from space. The AD and APD exhibit satisfactory values, with APD= 16% and AD 0.0006 at 550 nm for example, in comparison to similar studies [18, 19]. On the other hand, the APD values show an increasing dispersion of the comparison in respect to the decreasing wavelengths. That dispersion is particularly large at 412 nm. Although this is consistent with the known behavior of the atmospheric correction uncertainties, which increase from the red to the blue wavelengths, further analysis are needed to quantify these effects; such a study is one of the continuing objectives of this work. The overall results presented for the LISCO R_{rs} data are consistent with those obtained from similar validation exercises for coastal waters [18, 19] and to a lesser extent for open seas [1, 3]. It can therefore be concluded that LISCO site is representative and appropriate to serve as a key element of the AERONET-OC network for calibration/validation activities of satellite-derived parameters in coastal water area. It should be noted that the satisfactory comparison between HYPERSAS and satellite datasets enables to carry out validation of any satellite mission whatever the centers and widths of its spectral bands by integrating over the appropriate range of hyperspectral measurements made by HYPERSAS.

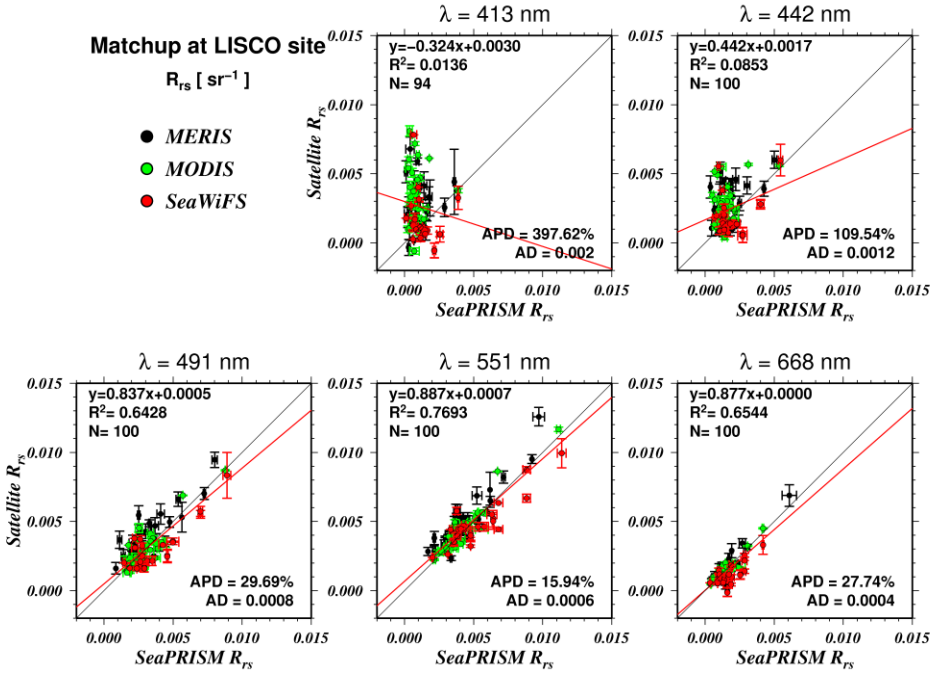

Figure 7. Scatter plots of the MERIS, MODIS and SeaWiFS match-ups with SEAPRISM normalized water-leaving radiance R_{rs} in sr^{-1} at 413, 442, 491, 551 and 668 nm. The vertical bars correspond to ± 1 the standard deviation due to the pixel heterogeneity. N is the total number of points for each spectral match-up; r is correlation coefficient; APD and AD are the absolute percentage difference and the absolute difference, respectively. The red line is regression line.

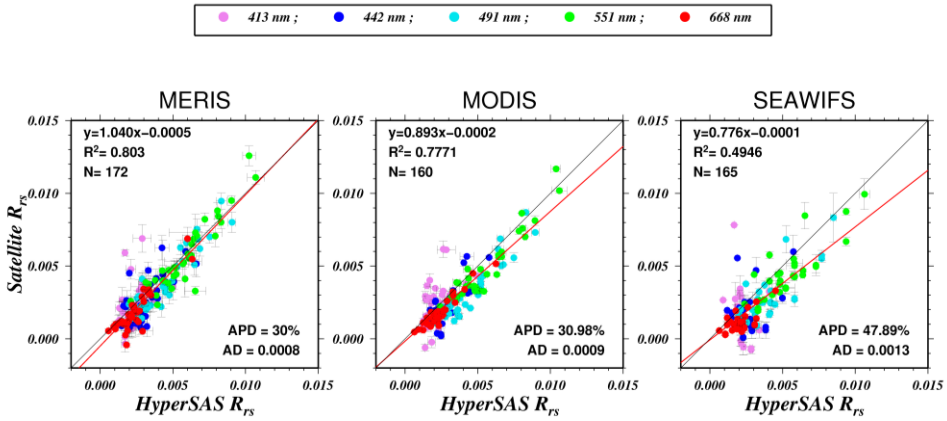

Figure 8. Matchup plots of the remote sensing reflectance, R_{rs} in [sr-1], derived from the three main OCR satellite versus R_{rs} derived from the HyperSAS measurement at LISCO site.

6 *Hyperspectral HICO imagery validation*

The Hyperspectral Imager for the Coastal Ocean[20, 21] (HICO) is the first spaceborne hyperspectral sensor designed specifically for the coastal ocean and estuarial, riverine, or other shallow-water areas. The HICO generates hyperspectral images, primarily over the 400–900nm spectral range, with a ground sample distance of ≈90m (at nadir) and a high signal-to-noise ratio. The HICO is now operating on the International Space Station (ISS). Its cross-track and along-track fields of view are 42km (at nadir) and 192 km, respectively, for a total scene area of 8000km^2.

The demonstrated accuracy of the hyperspectral HyperSAS data of LISCO is therefore extremely valuable to validate, and calibrate, the HICO sensor. The HICO data accuracy is here tested against HyperSAS data. The HICO image over LISCO area acquired the January 18th 2010 has been used for this preliminary data validation. This image is mostly cloud free, see Figure 9, and correspond to clear atmosphere conditions with AOT < 0.05 as measured by the AERONET system of LISCO site.

The level 1 HICO image has been corrected for the atmospheric radiance by the QUick Atmospheric Correction (QUAC) of the ENVI software. It should be noted that this QUAC algorithm is correcting for the atmospheric path radiance only and not the sea surface component of the radiance. Then, the HICO spectra have been extracted and averaged over a 6 × 6 pixel box corresponding to a 600 m × 600 m target area. The HyperSAS R_{rs} as well as the HICO corrected reflectance are presented in Figure 10. In this figure, the sum of the HyperSAS water-leaving and sea surface components of reflectance is also added to facilitate the comparison with the equivalent HICO data. Preliminary comparisons with a basic atmospheric correction show satisfactory HICO data consistency with HyperSAS data. Needs to pursue comparison with more accurate atmospheric correction such as tafkaa correction[22] coupled with AERONET-OC data at LISCO site in order to address the vicarious calibration of HICO based on HyperSAS database

Figure 9. False color HICO image over LISCO site from Level 1 image of the January 18th 2010.

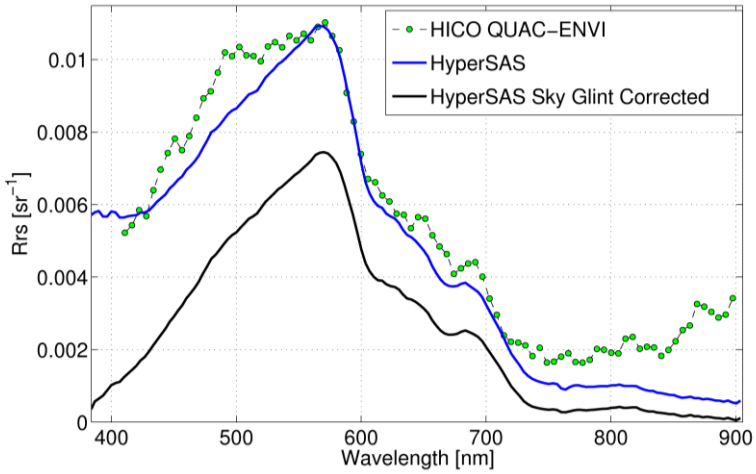

Figure 10. Spectra of the HyperSAS remote sensing reflectance (in black), sum of the HyperSAS water-leaving and sea surface components of reflectance (in blue) and the atmospheric corrected HICO reflectance of the January 18th 2010 measurements.

7 Summary and Conclusion

The focus of this study was primarily to assess the validity of collocated above-water multi and hyperspectral radiometric instrumentation to accurately measure the water-leaving radiance with a view to support calibration/validation activities for satellite derived parameters in coastal areas at the Long Island Sound Coastal Observatory location. The specific features of the LISCO instrumentation as well as those of the local water quality were detailed. The data quality process, developed for HyperSAS, has been described in detail and correlated with 1-year LISCO data statistics. The intrinsic uncertainty of HyperSAS data has been shown to be lower than 5% for a large spectral range, namely from 340 to 740 nm and a time range depending on the season of the year and more specifically to the sun elevation at the solar noon.

Based on this HyperSAS data quality assessment, the more than one year HyperSAS and SeaPRISM time series measurements of LISCO were presented and analyzed. The LISCO data were qualitatively and quantitatively validated on the basis of the temporal and spectral shape agreement of the retrieved normalized water-leaving radiances. The intercomparison exercise also showed that the overall uncertainty of the retrieved exact normalized water-leaving radiances is 19.5% with a positive bias of about 0.09. However, the HyperSAS and SeaPRISM datasets are strongly correlated for the central wavelengths from 442 to 668 nm (R^2>0.93) and to a lesser extent for the 412 nm band (R^2>0.76) with the slope of the regression lines close to one. In conclusion, the consistency between HyperSAS and SeaPRISM data retrievals has been demonstrated over one whole year of measurements with varying environmental conditions, including strong winds.

The LISCO data were used to validate the three main ocean color satellite sensors: MERIS, MODIS and SeaWiFS. Strong correlation and acceptable dispersion, comparable to the results others recent studies, have been found between the satellite and both multispectral and hyperspectral LISCO data. It can therefore be concluded that LISCO site is representative and appropriate to serve as a key element of the AERONET-OC network for calibration/validation activities of satellite-derived parameters in coastal water area. It should be noted that the satisfactory comparison between HYPERSAS and satellite datasets enables to carry out validation of any satellite mission whatever the centers and widths of its spectral bands by integrating over the appropriate range of hyperspectral measurements made by HYPERSAS. Finally, the hyperspectral data of HICO, remotely sensed from space, were shown to be in a satisfactory agreement with the LISCO HyperSAS data satellite mission. This very preliminary result makes it possible to contemplate the wider use of LISCO to carry out Calibration/Validation activities for the HICO sensor.

ACKNOWLEDGEMENT

This work was partially supported by grants from the Office of Naval Research and the National Oceanographic and Atmospheric Administration. We would like to thank NASA AERONET team for SeaPRISM calibration, data

processing and support of the site operations. We are grateful to Dr. G. Zibordi for frequent advice during the installation of the SeaPRISM and data processing.

REFERENCES

[1] S. W. Bailey, and P. J. Werdell, "A multi-sensor approach for the on-orbit validation of ocean color satellite data products," Remote Sensing of Environment, 102(1-2), 12 (2006).

[2] D. K. Clark, M. A. Yarbrough, M. E. Feinholz *et al.*, "MOBY, a radiometric buoy for performance monitoring and vicarious calibration of satellite ocean color sensors: Measurement and data analysis protocols," Ocean Optics Protocols for Satellite Ocean Color Sensor Validation, Revision, 4, 2003-211621 (2003).

[3] D. Antoine, F. d'Ortenzio, S. B. Hooker *et al.*, "Assessment of uncertainty in the ocean reflectance determined by three satellite ocean color sensors (MERIS, SeaWiFS and MODIS-A) at an offshore site in the Mediterranean Sea (BOUSSOLE project)," J. Geophys. Res., 113, (2008).

[4] G. Zibordi, B. N. Holben, I. Slutsker *et al.*, "AERONET-OC: a network for the validation of ocean color primary radiometric products," J. Atmos. Ocean. Technol, 26, 1634–1651 (2009).

[5] S. B. Hooker, G. Lazin, G. Zibordi *et al.*, "An evaluation of above-and in-water methods for determining water-leaving radiances," Journal of Atmospheric and Oceanic Technology, 19(4), (2002).

[6] G. Zibordi, F. Mélin, S. B. Hooker *et al.*, "An autonomous above-water system for the validation of ocean color radiance data," IEEE Transactions on Geoscience and Remote Sensing, 42(2), 401-415 (2004).

[7] S. Hlaing, T. Harmel, A. Ibrahim *et al.*, "Validation of ocean color satellite sensors using coastal observational platform in Long Island Sound." 7825, 782504.

[8] A. Tonizzo, T. Harmel, A. Ibrahim *et al.*, "Sensitivity of the above water polarized reflectance to the water composition." 7825, 78250F.

[9] G. Zibordi, S. B. Hooker, J. F. Berthon *et al.*, "Autonomous above-water radiance measurements from an offshore platform: a field assessment experiment," Journal of Atmospheric and Oceanic Technology, 19(5), (2002).

[10] T. Harmel, A. Gilerson, S. Hlaing *et al.*, "Long Island Sound Coastal Observatory (Part 1): Assessment of Above-water Measurement Uncertainties Using Collocated Multi and Hyper-spectral Sensors," Applied Optics, (2011, In Rev.).

[11] D. A. Aurin, H. M. Dierssen, M. S. Twardowski *et al.*, "Optical complexity in Long Island Sound and implications for coastal ocean color remote sensing," Journal of Geophysical Research, 115(C7), C07011 (2010).

[12] B. N. Holben, and e. al., "AERONET-A Federated Instrument Network and Data Archive for Aerosol Characterization," Remote sensing of environment, 66, 1-16 (1998).

[13] C. D. Mobley, "Estimation of the remote-sensing reflectance from above-surface measurements," Applied Optics, 38(36), 7442-7455 (1999).

[14] O. Dubovik, and M. D. King, "A flexible inversion algorithm for retrieval of aerosol optical properties from Sun and sky radiance measurements," J. Geophys. Res., 105(D16), 20,673-20,696 (2000).

[15] H. R. Gordon, and D. K. Clark, "Clear water radiances for atmospheric correction of coastal zone color scanner imagery," Applied Optics, 20(24), 4175-4180 (1981).

[16] A. Morel, and B. Gentili, "Diffuse reflectance of oceanic waters. III. Implication of bidirectionality for the remote-sensing problem," Applied Optics, 35(24), 4850-4862 (1996).

[17] Z. Lee, K. L. Carder, S. K. Hawes *et al.*, "Model for interpretation of hyperspectral remote-sensing reflectance," Applied Optics, 33(24), 5721-5732 (1994).

[18] G. Zibordi, J. F. Berthon, F. Mélin *et al.*, "Validation of satellite ocean color primary products at optically complex coastal sites: northern Adriatic Sea, northern Baltic Proper and Gulf of Finland," Remote Sensing of Environment, (2009).

[19] C. Jamet, H. Loisel, C. P. Kuchinke *et al.*, "Comparison of three SeaWiFS atmospheric correction algorithms for turbid waters using AERONET-OC measurements," Remote Sensing of Environment, In Press, Corrected Proof, (2011).

[20] R. L. Lucke, M. Corson, N. R. McGlothlin *et al.*, "Hyperspectral Imager for the Coastal Ocean: instrument description and first images," Appl. Opt., 50(11), 1501 (2011).

[21] C. Davis, J. Bowles, R. Leathers *et al.*, "Ocean PHILLS hyperspectral imager: design, characterization, and calibration," Opt. Express, 10(4), 210 (2002).

[22] B. C. Gao, M. J. Montes, Z. Ahmad *et al.*, "Atmospheric correction algorithm for hyperspectral remote sensing of ocean color from space," Applied Optics, 39(6), 887-896 (2000).